Available online at www.sciencedirect.com
SCIENCE DIRECT®

Journal of the European Ceramic Society 24 (2004) 2339–2347
www.elsevier.com/locate/jeurceramsoc

Thermal shock resistance of fibrous monolithic Si_3N_4/BN ceramics

Young-Hag Koh[a,b,*], Hae-Won Kim[a], Hyoun-Ee Kim[a], John W. Halloran[b]

[a]*School of Materials Science and Engineering, Seoul National University, Seoul, 151-742, South Korea*
[b]*Materials Science and Engineering Department, University of Michigan, Ann Arbor, MI 48109-2136, USA*

Received 15 January 2003; received in revised form 25 June 2003; accepted 6 July 2003

Abstract

Thermal shock resistance of fibrous monolithic Si_3N_4/BN ceramic was investigated by measuring the strength retention after varying the temperature difference (ΔT) up to 1400 °C and was compared with that of monolithic Si_3N_4. Monolithic Si_3N_4 showed catastrophic drop in flexural strength above ΔT of 1000 °C, while FM showed negligible reduction in flexural strength without critical temperature difference (ΔT_c). Two parameters, such as the resistance to crack initiation (R') and crack propagation (R''''), were used in order to explain the thermal shock behaviors of fibrous monolith and monolithic Si_3N_4. Furthermore, crack interactions during flexural testing, such as delamination cracks and crack deflection, were characterized and were related to the work-of-fracture (WOF).

Keywords: BN; Composites; Fibrous monoliths; Si_3N_4; Thermal shock

1. Introduction

Fibrous monoliths have been regarded as promising materials for structural applications because of the noncatastrophic failure due to its unique architecture.[1–7] Fibrous monoliths are sintered or hot-pressed monolithic ceramics with a distinct fibrous texture consisting of strong cell and weak cell boundary that act as a easy crack path.[1] One of the most promising fibrous monoliths for high temperature applications is Si_3N_4/BN system because of its high strength and oxidation resistance at elevated temperature.[4–7]

Since these composite materials are candidates as the high-temperature applications (e.g. in gas turbine engines), it is inevitable to involve some kind of thermal shock loading. Most ceramics showed catastrophic drops in mechanical properties, such as flexural strength, elastic modulus, after thermal shock above the critical temperature (ΔT_c).[11–15] This catastrophic drop in mechanical properties after thermal shock have limited the wide applications at high-temperatures.

Thermal shock resistance is dependent on several primary mechanical properties, such as fracture toughness, fracture behavior, fracture strength, elastic modulus and coefficient of thermal expansion of material.[11,12] Hence, there are some possible methods to increase the thermal shock resistance of materials. For example, the addition of ductile secondary phase into Al_2O_3 matrix increases the thermal shock resistance due to both reduced elastic modulus and increased fracture toughness.[14] Also, flaw-tolerant material, such as fiber (or whisker)-reinforced ceramics and laminated ceramics shows excellent thermal shock resistance due to the increased resistance to crack propagation through crack interactions with toughening agents (fiber, whisker and weak interface).[16–18] However, so far, in spite of its importance for high temperature applications, no research has been done on thermal shock resistance of fibrous monolith.

In this paper, we have investigated thermal shock resistance of fibrous monolithic Si_3N_4/BN ceramics with temperature difference ranging from 800 to 1400 °C, by measuring the retention of mechanical properties, such as flexural strength and work-of-fracture (WOF). For the purpose of comparison, monolithic Si_3N_4 was also tested under the same conditions.

2. Experimental

2.1. Billet fabrication

Fibrous monolithic Si_3N_4/BN ceramic was fabricated using coextrusion process to produce a structure with

* Corresponding author.
E-mail address: younghag@engin.umich.edu (Y.-H. Koh).

0955-2219/$ - see front matter © 2003 Elsevier Ltd. All rights reserved.
doi:10.1016/S0955-2219(03)00644-7

uniaxially aligned ~250 micron cells of composition Si_3N_4 (E-10, Ube Industries, Tokyo, Japan) with 6 wt.% Y_2O_3 (99.9%, Johnson Matthey Electronics, MA, USA) and 2 wt.% Al_2O_3 (HP-DBM, Reynolds, Bauxite, AK, USA), separated by 15~25 micron boron nitride (HCP, Advanced Ceramics Corp., Cleveland, OH, USA) cell boundaries. Further details on the fabrication of fibrous monoliths are described elsewhere.[1,4] For comparison, monolithic Si_3N_4 with 6 wt.% Y_2O_3 and 2 wt.% Al_2O_3 as sintering aids was also fabricated. The green billets were hot-pressed at 1740 °C under an applied pressure of 25 MPa for 2 h in a flowing N_2 atmosphere. The density of the specimens was measured using the Archimedes method and the theoretical density of the specimens was estimated by the rule of mixture.

2.2. Specimen preparation

The thermal shock resistance was determined by measuring the retention of the flexural strength of water-quenched specimen. Specimens were machined into a bar shape with dimensions of 3×4×45 mm and ground with a 600-grit diamond wheel. The tensile side of the specimens was polished using diamond paste down to 3 μm, and subsequently chamfered to minimize machining flaws. Also, the side surfaces of each specimen were polished down to 30 μm.

2.3. Thermal shock test

Thermal shock test was carried out in a vertical tube furnace at temperatures between 800 °C and 1400 °C in laboratory air. The furnace was heated at a heating rate of 10 °C/min and maintained at exposure temperatures. Polished specimens, suspended at the end of a platinum wire, were inserted into the hot-zone from the top and were soaked for 30 min to induce the homogeneous temperature distribution. After exposure, the specimens were quickly dropped into the water bath with a capacity of 5000 cc. The temperature of water bath did not increase notably after dropping the specimen.

2.4. Mechanical test and characterization

The flexural strength after thermal shock test was measured at room temperature by a four-point flexural configuration at a cross-head speed of 0.5 mm/min, and inner- and outer-spans of 20 and 40 mm, respectively. The load versus crosshead deflection response and the work of fracture, calculated by determining the area under the load–crosshead deflection curve and dividing it by twice the cross-sectional area of the sample, are reported. Also, crack propagation during flexural strength test after thermal shock was observed by an optical microscope and an SEM microscope. Elastic moduli were measured by the impulse technique using a commercially available tester (Grindo-sonic model MK4x, J. W. Lemmon, St, Louis, MO, USA).[20]

3. Results

3.1. Microstructure and mechanical properties before thermal shock

The typical microstructure of fibrous monolithic Si_3N_4/BN ceramic (FM) is shown in Fig. 1. Low magnification SEM micrographs of polished sections, shows three-dimensional representations of the sub-millimeter structure of fibrous monoliths. The polycrystalline silicon nitride cells appear in dark contrast, while the continuous boron nitride cell boundaries appear in bright contrast. The Si_3N_4 cells are surrounded by the cell boundaries consisting of BN particles bonded with yttriumaluminosilicate.

The mechanical properties of monolithic Si_3N_4 and FM samples are summarized in Table 1. For FM, the measured density (ρ) was slightly higher than theoretical value (based on 82.5 vol.% Si_3N_4 cells and 17.5 vol.% BN cell boundaries for fibrous monoliths), implying full densification of both Si_3N_4 cell and BN cell boundary materials occurred. Elastic modulus (E) and flexural strength (MOR) of FM were slightly lower than those of monolithic Si_3N_4, while apparent WOF increased remarkably due to the noncatastrophic failure through extensive crack interactions along the weak BN cell boundaries.

The typical flexural responses of monolithic Si_3N_4 and FM are shown in Fig. 2. As expected, monolithic Si_3N_4 showed higher strength but negligible apparent WOF

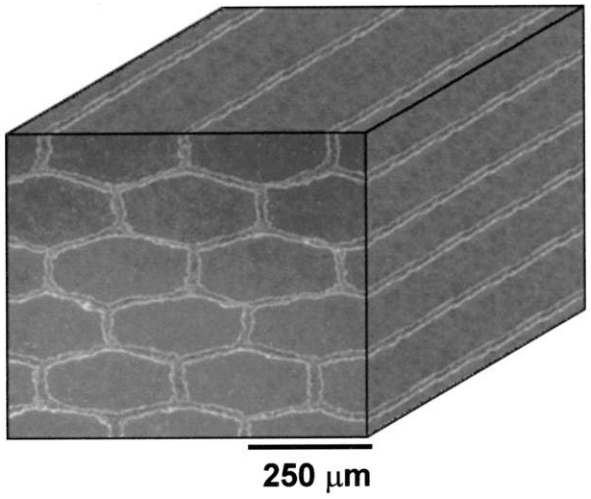

Fig. 1. Low magnification SEM micrographs of polished sections, shows three-dimensional representations of the submillimeter structure of fibrous monoliths. The polycrystalline silicon nitride cells appear in dark contrast and the continuous boron nitride cell boundaries are in bright contrast. (Courtesy of Bruce King).

because of catastrophic failure [Fig. 2(A)]. On the other hand, FM exhibited noncatastrophic failure due to its unique architecture, comprised of strong Si_3N_4 cell and weak BN cell boundary, resulting in high apparent WOF [Fig. 2(B)]. Moreover, the apparent strength retention after the first failure was above 50% of original strength, showing the noncatastrophic. This noncatastrophic nature was attributed to the extensive crack interactions, such as crack delaminations and crack deflections, as shown in Fig. 3. For fibrous monoliths, the crack propagates through the weak cell boundaries to reduce the applied stress. Similar crack propagations have been observed in many different kinds of fibrous monoliths.[1–5]

3.2. Mechanical properties after thermal shock

When a material (monolithic Si_3N_4 or FM) is subjected to a rapid decrease in temperature (ΔT), the surface of the component is placed under tension and the interior under compression. If the tensile stress developed on the surface exceeds the strength of the material, the cracks are generated, leading to a rapid drop in flexural strength.[11–15]

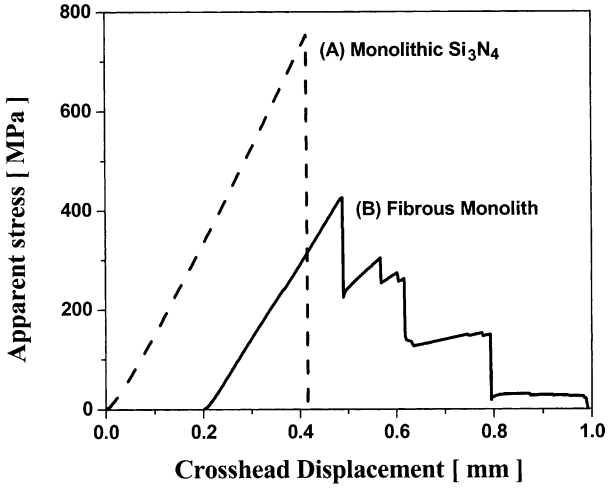

Fig. 2. Flexural response of (A) monolithic Si_3N_4 and (B) fibrous monolithic Si_3N_4/BN ceramic before thermal shock test. Monolithic Si_3N_4 showed brittle fracture, while fibrous monolith showed graceful fracture due to unique architecture. Note, retained apparent stress after first drop is above 50% (B).

Table 1
Summarized mechanical properties of monolithic Si_3N_4 and fibrous monolithic Si_3N_4/BN ceramic

Samples	ρ (g/cc)	E (GPa)	MOR (MPa)	WOF (kJ/m^2)
Monolithic Si_3N_4	3.27±0.1	318±4	832±46	Negligible
Fibrous monolith	3.09±0.1	276±3	416±34	5.94±1.34

3.2.1. Strength retention

The thermal shock resistance was observed by measuring the retention of the flexural strength after thermal shock test, as shown in Fig. 4. For monolithic Si_3N_4, the traditional thermal shock behavior of brittle material was observed, that is, the flexural strength decreased rapidly after thermal shock with temperature difference of 1000 °C [Fig. 4(A)]. However, the flexural strength of FM after thermal shock test was not changed much [Fig. 4(B)], showing the excellent thermal shock resistance. Moreover, there was no critical temperature (ΔT_c), at which the strength decreases catastrophically, up to 1400 °C.

3.2.2. Fracture behavior

After thermal shock, the fracture behaviors of monolithic Si_3N_4 and FM were not basically changed, as

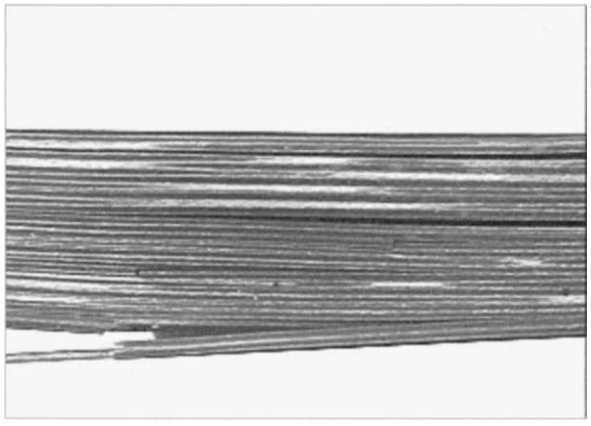

Fig. 3. Optical photograph of crack propagation of the fibrous monolithic Si_3N_4/BN ceramic after flexural testing. Extensive crack interactions, such as crack delamination and crack deflection, were observed.

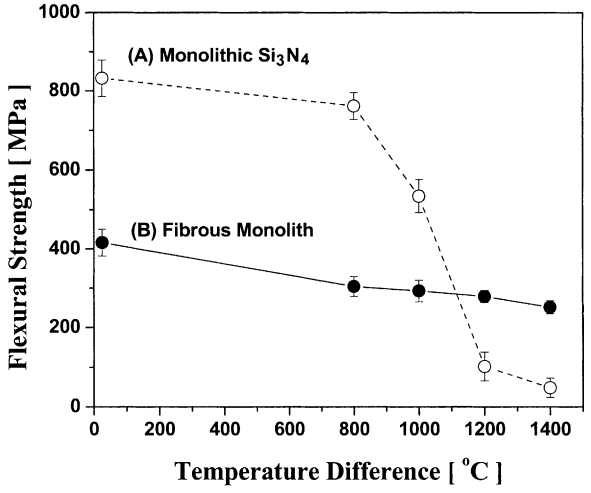

Fig. 4. Flexural strength of (A) monolithic Si_3N_4 and (B) fibrous monolithic Si_3N_4/BN ceramic after thermal shock with temperature difference (ΔT). Flexural strength of monolithic Si_3N_4 reduced catastrophically after thermal shock with $\Delta T = 1000$ °C; however, fibrous monolith showed negligible decrease in flexural strength.

shown in Fig. 5, that is, monolithic Si_3N_4 showed catastrophic failure (not shown), while FM showed noncatastrophic failure regardless of temperature difference. Furthermore, with the increase in temperature difference, more extensive crack interactions were observed. The increase in apparent stress after fist drop implies the midplane shear stress after thermal shock.

The apparent WOF of the FM specimens increased remarkably after thermal shock test, as shown in Fig. 6. The WOF is higher if there is a large retained load once fracture begins, and strongly depends upon the extent of crack interactions and delamination. The thermally shocked specimens exhibited higher retained strength and extensive crack delamination. Thermal shock damage seems to be absorbed within the BN cell boundaries, which would decrease the cell boundary fracture resistance, enabling easier crack deflection and higher WOF.

3.2.3. Crack propagation

The increased crack interactions in the thermally shocked sample, manifested by crack path, are clearly shown in Fig. 7A–D. After thermal shock, crack interactions (crack delamination and crack deflection) occurred more extensively compared to the specimen before the thermal shock (Fig. 3). Pronounced crack delamination occurred by the thermal shock of 800 °C [Fig. 7(A)], and further long crack delamination was observed after the thermal shock of 1200 °C [Fig. 7 (C)]. The tendency for crack delamination in FM ceramics is influenced by the interfacial crack resistance of the BN-containing cell boundary.[7,8] The increase in WOF after thermal shock suggests that thermal shock reduces the interfacial crack resistance of the cell boundary, which is a composite of boron nitride and glass. The BN particles in the as-hot pressed material are already microcracked.[1] Hence, thermal shock damage seems to be absorbed within the BN cell boundaries, which would decrease the cell boundary fracture resistance, enabling easier crack deflection and higher WOF. The specimens shocked with the highest temperature difference ($\Delta T = 1400$ °C) had the most extensive crack delaminations, as shown in Fig. 7(D). This remarkable increase in crack delamination is attributed to not only preferential crack propagation caused by thermal stress but also oxidized damage layer during exposure to air.

The change of surface morphology after thermal shock test is shown in Fig. 8. Up to the temperature difference of 1200 °C, the surface was not damaged (not shown). However, with temperature difference of 1400 °C, the surface (both BN cell boundary and Si_3N_4 cell) was damaged to some extent due to the oxidation.

3.2.4. Load-bearing capacity

The thermal stress developed on surface and interface of Si_3N_4 and BN after the thermal shock affected the flexural response of FM upon subsequent room temperature testing, as shown in Fig. 9. The retained strength after the fist drop (1st drop/1st peak) was not basically changed within the range between 40% and 55%, meaning the excellent load-bearing capacity for actual applications. However, the normalized maximum strength (2nd peak/1st peak) increased after thermal shock test. This result means that the first peak was caused by the crack initiation on the surface; thus, the surface was slightly weakened due to the thermal stress. Furthermore, the thermal stress developed in interface of Si_3N_4 and BN promoted extensive crack interactions, resulting in increased WOF.

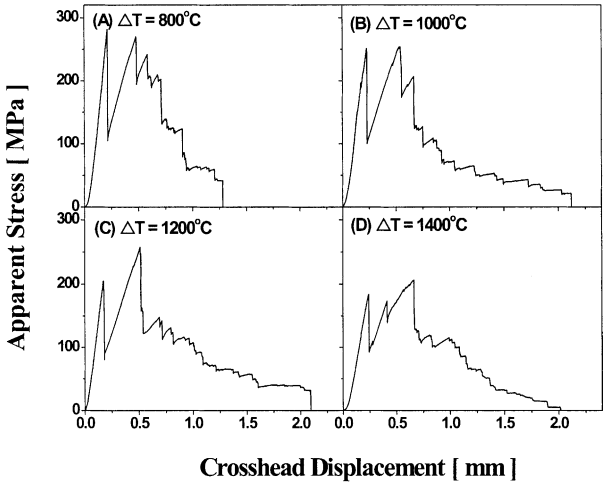

Fig. 5. Flexural responses of fibrous monolithic Si_3N_4/BN ceramic after thermal shock with temperature difference (ΔT) of (A) 800 °C, (B) 1000 °C, (C) 1200 °C, and (D) 1400 °C. All samples exhibited graceful fractures.

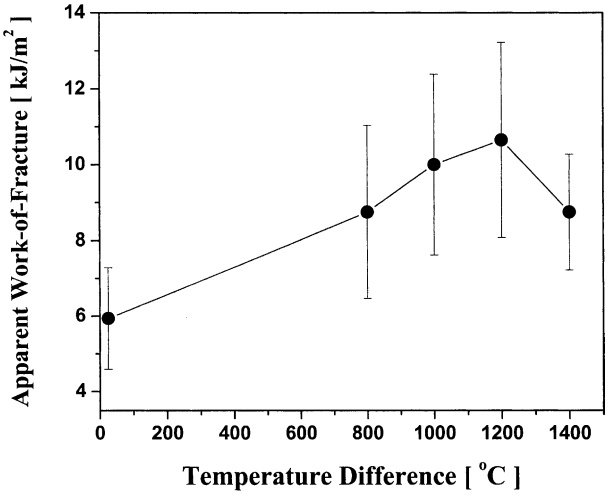

Fig. 6. Work-of-fracture (WOF) of fibrous monolithic Si_3N_4/BN ceramic after thermal shock with temperature difference (ΔT). Fibrous monolith exhibited significant WOF due to extensive crack interactions.

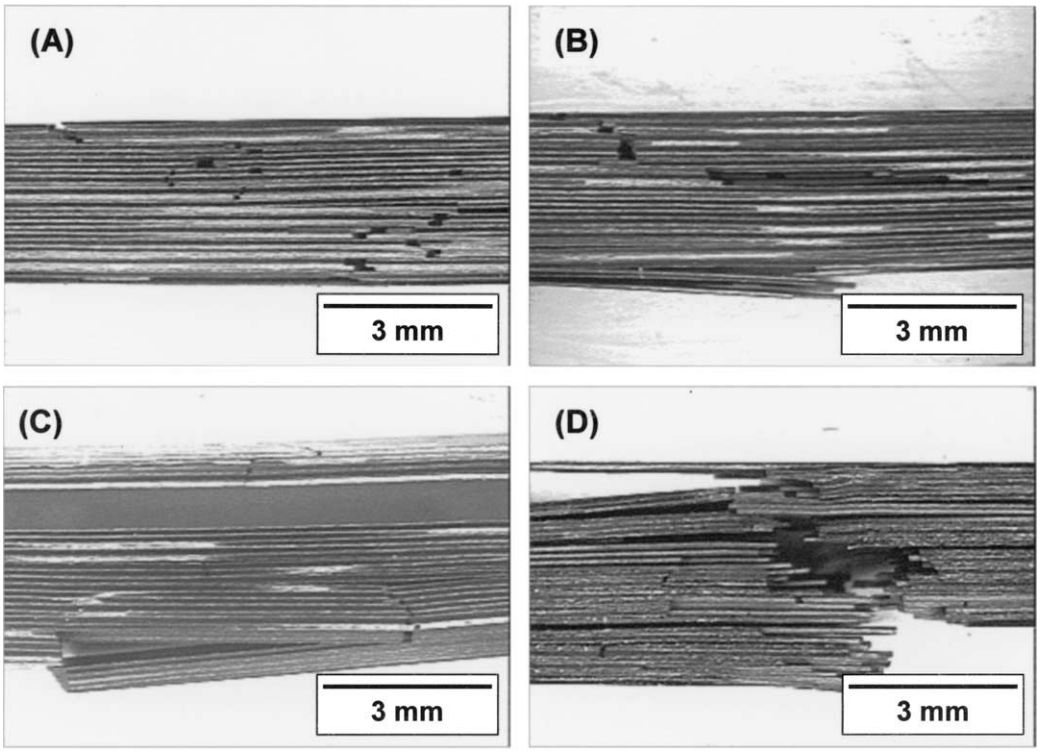

Fig. 7. Optical photographs of crack propagation of fibrous monolithic Si_3N_4/BN ceramic after thermal shock with temperature difference (ΔT) of (A) 800 °C, (B) 1000 °C, (C) 1200 °C, and (D) 1400 °C during flexural testing. All samples showed extensive crack interactions, such as crack delaminations and crack deflections.

4. Discussion

The fracture strength of thermally shocked monolithic Si_3N_4 is strongly dependent on the magnitude of tensile stress developed on the surface, that is, if the tensile stress exceeds its strength, the cracks are generated on the surface, resulting in catastrophic drop in flexural strength. However, for FM sample, the fracture strength of FM sample is less sensitive to surface flaws; therefore, the resistance to crack propagation is a more critical factor than the resistance to crack initiation, which is critical for brittle monolithic Si_3N_4. However, pre-existing cracks on BN cell boundaries after hot-pressing ($T = 1740$ °C) also affects the flexural response, resulting in crack interactions. Therefore, some factors, such as the magnitude of thermal stress on surface, thermal shock resistance parameter and pre-existing cracks, are discussed.

4.1. Magnitude of thermal stress on the surface (σ_{TS})

Considering the structure of this uniaxial FM (Fig. 1), it is noted that the elastic modulus and thermal expansion coefficient is different in the transverse and longitudinal directions. In addition, the hexagonal BN is strongly textured,[19] with the high stiffness/low expansion *a*-axis aligned preferentially in the longitudinal direction and the lower stiffness/higher expansion *c*-axis aligned in the transverse direction. Therefore mechanical properties, such as elastic modulus, coefficient of thermal expansion (CTE) and Poisson's ratio, of FM sample show anisotropy, as described in Table 2.

The elastic modulus of monolithic silicon nitride was significantly higher, and the transverse modulus of the FM was less than half the longitudinal modulus, due to the BN, which has a small *c*-axis modulus. The longitudinal thermal expansion of the FM was slightly less than monolithic silicon nitride, decreased by the a-axis BN, while the transverse thermal expansion of the FM was much larger, increased by the *c*-axis BN. Poisson's ratios were estimated from rule-of-mixture by taking 0.27 and 0.2 for Si_3N_4[21] and BN,[22] respectively.

The magnitude of thermal stress induced by the same exposure will be different, depending on the cell alignment (longitudinal and transverse direction). The traditional approach to evaluate the thermal shock resistance is based on quenching the specimen from an elevated temperature into a quenching media and measuring the fracture strength of the material. Neglecting the heat transfer and size effects, the maximum tensile stress (σ_{TS}) generated on the surface of the specimen can be calculated according to:[11]

$$\sigma_{TS} = (E\alpha/(1-\nu)) \cdot \Delta T \quad (1)$$

where E, α and ν represent the elastic modulus, the coefficient of thermal expansion (CTE) and Poisson's

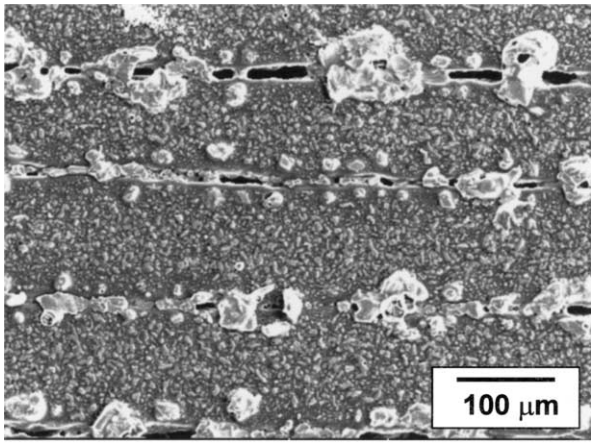

Fig. 8. SEM micrograph of fibrous monolithic Si_3N_4/BN ceramic after thermal shock with temperature difference (ΔT) of 1400 °C. After exposure at temperature up to 1200 °C, the surface was not damaged, while after exposure at 1400 °C, the surface layer was damaged by the oxidation of both BN cell boundaries and Si_3N_4 cell material.

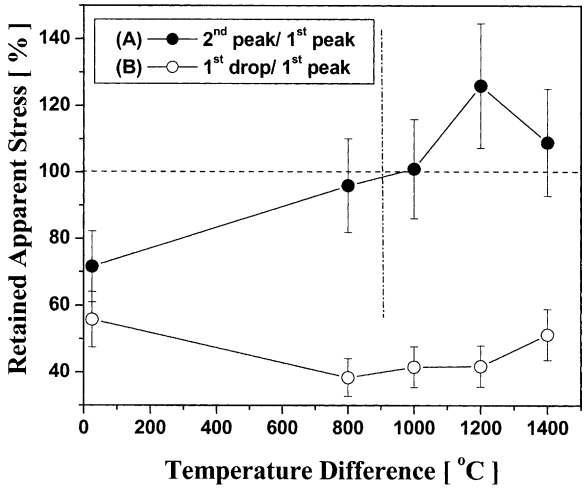

Fig. 9. Retained apparent strength of fibrous monolithic Si_3N_4/BN ceramics; (A) 2nd peak/1st peak and (B) 1st drop /1st peak from load–deflection curve. After thermal shock, the retained strength of 2nd peak/1st peak increased, implying that the fracture initiated from surface defects generated by thermal shock. Note, the retained strengths after first drop (B) of the all samples are higher than 40%, suggesting excellent load-bearing capacity.

ratio, respectively. ΔT is the temperature difference between exposure and water temperature.

The normalized thermal stresses ($\sigma_{N,TS}$), that is, thermal stresses with longitudinal and transverse direction were divided by that of monolithic Si_3N_4, are estimated, as described in Table 2. Lower tensile stresses were developed on the surface of FM samples with 80 and 55% for longitudinal and transverse direction, respectively. Considering temperature difference of 1200 °C, the tensile stress of ~2000 MPa was developed on the surface of monolithic Si_3N_4; this value is high enough to develop the cracks on the surface, resulting in catastrophic drop in flexural strength [Fig. 4(A)]. However, actual thermal stress needs consideration of the heat transfer depending on heat transfer coefficient of the quenching medium, the thermal conductivity (k) and the characteristic dimension of the sample. Moreover, the value from Eq. (1) only suggests the condition for crack initiation which is critical for brittle material (i.e., monolithic Si_3N_4) and not for crack propagation, which is more important for tough material (i.e., FM sample). Therefore, a new parameter for describing thermal shock resistance should be considered.

Table 2
The values for calculating the normalized thermal stress ($\sigma_{N,TS}$) developed on the surface of monolithic Si_3N_4 and fibrous monolithic Si_3N_4/BN ceramic

Samples	E (GPa)	ν	α (10^{-6}/°C)	$\sigma_{N,TS}$
Monolithic Si_3N_4	318	0.27	4	1
Fibrous monolith (longitudinal)	276	0.25	3.8	0.80
Fibrous monolith (transverse)	127	0.12	6.7	0.55

4.2. Thermal shock resistance parameter

The conditions for crack initiation and propagation have been extensively analysed by Hasselman et al.[11,12] Opposing property requirements prevail, depending on whether the material is required to be resistant to crack initiation (for which high strength and low stiffness are essential) or resistant to strength degradation following a severe thermal shock (in which case low strength and high stiffness are beneficial). We consider the crack initiation parameter R' and crack propagation parameter R'''' estimated for monolithic Si_3N_4 and FM sample consisting only longitudinal direction despite there was anisotropy in thermal stress. These parameters can be expressed as

$$R' = k \cdot \sigma_f(1-\nu)/(E\alpha) \tag{2}$$

$$R'''' = K_{IC}^2/\left(\sigma_f^2 \cdot (1\text{-}\nu)\right) \tag{3}$$

where, σ_f is the fracture strength and K_{IC} is the toughness and k is the thermal conductivity of the material. The fracture strength of monolithic Si_3N_4 is almost twice that of FM sample (Table 1). The thermal conductivities are 37 and 53 W/m K for monolithic Si_3N_4 and FM sample with longitudinal direction. The calculated crack initiation parameter R' (17.7 kW/m) of monolithic Si_3N_4 is only slightly larger than that (15.8 kW/m) of FM sample, implying the condition for crack initiations are almost the same. Therefore, the large difference in behavior can not be explained by resistance to crack initiation. The toughness of FM sample was twice that of monolithic Si_3N_4.[23] The calculated crack

propagation parameter R'''' of FM sample is much larger (>16 times) than that of monolithic Si_3N_4, implying that the crack propagation is more restricted for FM sample, while the resistance to crack initiation is slightly lower than that of monolithic Si_3N_4.

Considering thermal shock parameters (R' and R''''), FM sample is expected to show excellent thermal shock resistance (see Fig. 4) because the resistance to crack propagation (R'''') is much higher, while the resistance to crack initiation (R') is slightly lower compared to monolithic Si_3N_4. Similar increased thermal shock resistance have been observed for layered ceramic structures where the cracks are deflected reliably at the interfaces.[16]

4.3. Pre-existing microcracks on BN cell boundaries

We have previously observed the generation of cracks within BN cell boundary layer after hot-pressing.[1] The CTE of BN in the basal plane is slightly negative from room temperature to 800 °C, about -2×10^{-6}/°C,[24] while, the CTE perpendicular to the basal plane is very large and positive, about $+40\times10^{-6}$/°C.[25] Therefore, the BN contracts perpendicular to the basal plane (i.e., in the [0001] direction) during cooling. If the surrounding Si_3N_4 grains or glassy phase constrain the BN platelets, large tensile stresses are developed perpendicular to the basal plane, resulting in separating BN platelets into layers along the basal plane direction. Thus the as-fabricated specimens (before the thermal shock treatment) had many pre-existing microcracks within the BN-rich cell boundary. The delaminated microcracks of the BN-rich cell boundaries, including the amount of the glass and the extent of pre-existing microcracks, determine the fracture resistance of the cell boundary (Γ_{BN}) and the tendency for the crack deflection and delamination.[8–10]

Furthermore, shear stresses developed parallel to the basal plane made the surface of the platelets slide relative to each other. Similarly, pre-existing microcracks were extended due to the anisotropy in CTE after thermal shock, dissipating the thermal stress; therefore, crack propagations through BN cell boundaries became more favorable, resulting in high WOF (see Figs. 5 and 7). Some researches have observed that pre-existing microcracks in BN platelets of Si_3N_4–BN and Al_2O_3–BN composites are beneficial to thermal shock resistance.[26,27]

4.4. Thermal shock induced cracks and crack propagation during subsequent flexural testing

After thermal shock, the FM sample is placed under transverse and longitudinal stress depending on the fiber alignment, as shown in Fig. 10(A). The flaw tolerant nature of the FM is related to crack deflection at the BN-rich cell boundaries. During thermal shock, the longitudinal thermal stress may fracture occasional Si_3N_4 cells, as shown in Fig. 10(B). The transverse thermal stress most likely causes localized extension of the pre-existing flaws in the BN-rich cell boundary and is unlikely to cause cracks within the Si_3N_4 cells. The postulated BN-cell boundary cracks could not be observed because they would be observed by the pre-existing cracks in the BN and the rough topography of the cell boundary region. However, the extension of BN-cell boundary cracks is believed to decreases the cell boundary fracture resistance (Γ_{BN}), which is consisted with the observation of more extensive delamination after flexural testing of severely shocked sample.

The degree of delamination cracks is significantly dependent on the magnitude of thermal stress due to thermal shock that can extend the pre-existing cracks in BN-rich cell boundary. The fraction of cell boundary delamination was calculated by counting the ratio of delaminated layers to the total number of cell boundary layer from the SEM micrographs, as shown in Fig. 11. Three cell boundaries (marked by arrows) were extensively delaminated and the rest one was remained without delamination crack. The degree of delamination cracks significantly increased after thermal shock, as shown in Fig. 12. Before thermal shock, 40% cell boundaries were delaminated. However, after thermal shock with a temperature difference of 1400 °C, almost every BN cell boundary was delaminated. These results are attributed the decrease in cell boundary fracture resistance (Γ_{BN}) through the extension of pre-existing

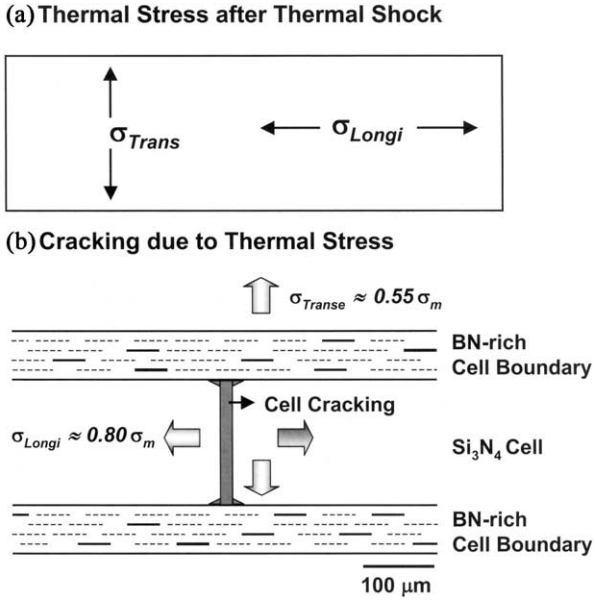

Fig. 10. (A) Thermal stress after thermal shock in transverse and longitudinal direction and (B) A schematic of single Si_3N_4 cell between two BN-rich cell boundaries, illustrating (i) pre-existing cracks in cell boundaries (- - -) and cell boundary cracks extended by thermal shock (—), (ii) possible transverse cracks in Si_3N_4 cell.

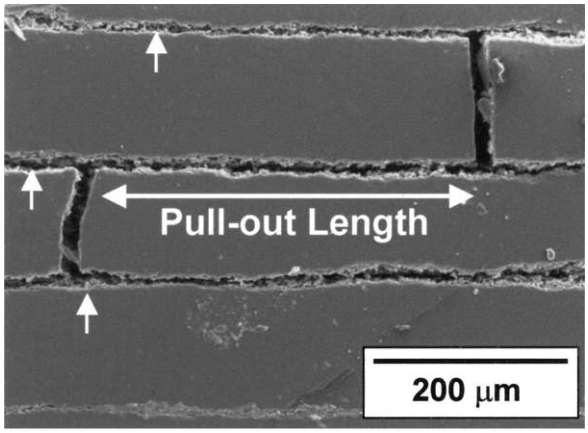

Fig. 11. SEM micrograph of the thermally shocked sample after flexural testing, illustrating the delamination cracks (marked by arrow) and pull-out length.

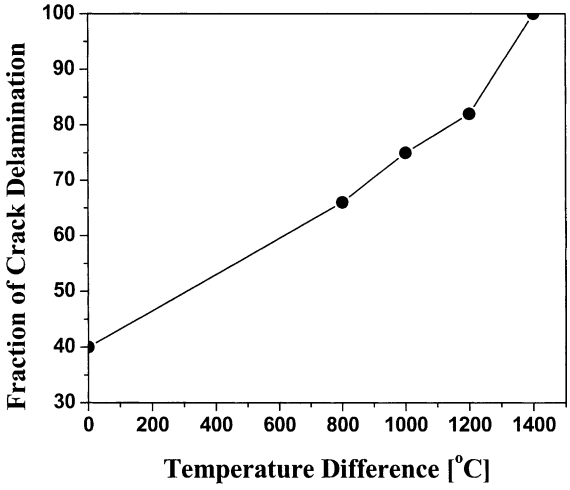

Fig. 12. Fraction of crack delamination in the thermally shocked sample after flexural testing as a function of temperature difference (ΔT). Temperature difference (ΔT) of 0 °C represents the sample before thermal shock.

cracks on BN-rich cell boundaries, consequently promoting the delamination cracks.

The magnitude of thermal stress is expected to change the length of the delamnination cracks; however, it is difficult to quantify the length of delamination cracks, because it is not easy to discern the crack tip in the BN-rich cell boundary. Therefore, the delamination distance, defined as pull-out length (see Fig. 11), can be measured from the distance between through-thickness cracks in adjacent Si_3N_4 layers. A cumulative distribution plot of pull-out lengths is shown in Fig. 13 for each of the samples before and after thermal shock. Before thermal shock, the FM sample showed the amounts of short pull-out length (<100 μm). Almost half of the delamination cracks kinked out of the BN cell boundary after propagating only a short distance. However, after thermal shock, the pull-out length was significantly increased, implying that the decrease in cell boundary

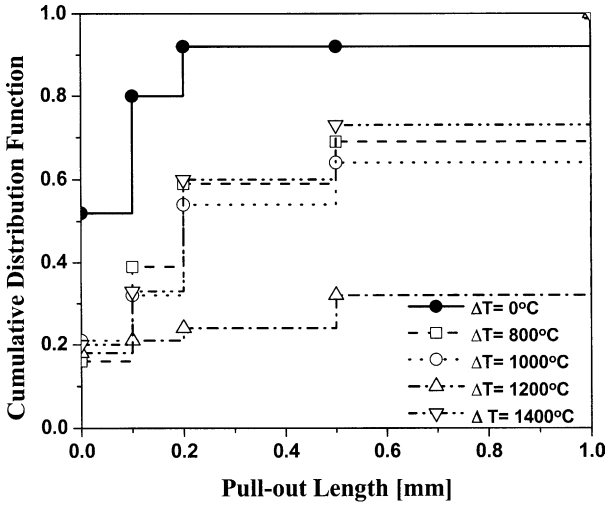

Fig. 13. Cumulative distribution function versus pull-out length of the samples before and after thermal shock with a various temperature difference (ΔT).

fracture resistance (Γ_{BN}). The FM samples after thermal shock with the temperature difference of 1200 °C, 70% of the delamination cracks showed the long pull-out length (>1000 μm). However, after thermal shock with the temperature difference of 1400 °C, the pull-out length was decreased again even tough almost every BN-rich cell boundary was delaminated (see Fig. 12). This result is attributed to the damage of both Si_3N_4 cells and BN cell boundaries due to the oxidation. In other words, when the Si_3N_4 cell is strong (i.e., few flaws on the surface), the delamination cracks extends to long distance before kinking out of BN-rich cell boundary. However, when the Si_3N_4 cell is damaged due to the oxidation (i.e., many flaws on the surface, see Fig. 8), amounts of the delamination cracks kink out of the BN-rich cell boundary after propagating only a short distance, in which the flaws are present on Si_3N_4 cell, while almost every cell boundary is delaminated due to the decrease in cell boundary fracture resistance.

5. Conclusions

Excellent thermal shock resistance was observed for fibrous monolithic Si_3N_4/BN ceramics. Monolithic Si_3N_4 showed a catastrophic drop in flexural strength with temperature difference of 1000 °C, meaning that the tensile stress was developed on the surface exceeding its fracture strength, and thus cracking the surface. However, fibrous monolithic showed negligible reduction in flexural strength, and remarkable increase in work-of-fracture (WOF). Such excellent thermal shock resistance was attributed to high resistance to crack propagation (R'''') through crack interactions with weak cell boundaries. The remarkable increase in WOF and delamination cracks were attributed to the reduction in

cell boundary fracture resistance by extension of pre-existing microcracks on BN-rich cell boundaries.

Acknowledgements

This research was supported by a grant from the Center for Advanced Materials Processing (CAMP) of the 21st Century Frontier R&D Program funded by the Ministry of Science and Technology, Republic of Korea.

References

1. Kovar, D., King, B. H., Trice, R. W. and Halloran, J. W., Fibrous monolithic ceramics. *J. Am. Ceram. Soc.*, 1997, **80**, 2471–2487.
2. Baskaran, S., Nunn, S. D., Popovic, D. and Halloran, J. H., Fibrous monolithic ceramics: I, fabrication, microstructure, and indentation behavior. *J. Am. Ceram. Soc.*, 1993, **76**, 2209–2216.
3. Baskaran, S. and Halloran, J. H., Fibrous monolithic ceramics: II, flexural strength and fracture behavior of the silicon carbide/graphite system. *J. Am. Ceram. Soc.*, 1993, **76**, 2217–2224.
4. King, B. H. *Influence of Architecture on the Mechanical Properties of Fibrous Monolithic Ceramics*. PhD thesis, University of Michigan, Ann Arbor, MI, 1997.
5. Trice, R. W. and Halloran, J. H., Effect of sintering aid composition on the processing of Si_3N_4/BN fibrous monolithic ceramics. *J. Am .Ceram. Soc.*, 1999, **82**, 2943–2947.
6. Trice, R. W. and Halloran, J. H., Elevated-temperature mechanical properties of silicon nitride/boron nitride fibrous monolithic ceramics. *J. Am. Ceram. Soc.*, 2000, **83**, 311–316.
7. Trice, R. W. and Halloran, J. H., Influence of microstructure and temperature on the interfacial fracture energy of silicon nitride/boron nitride fibrous monolithic ceramics. *J. Am. Ceram. Soc.*, 1999, **82**, 2502–2508.
8. Kovar, D., Thouless, M. D. and Halloran, J. H., Crack deflection and propagation in layered silicon nitride/boron nitride ceramics. *J. Am. Ceram. Soc.*, 1998, **81**, 1004–1012.
9. He, M. Y. and Hutchinson, J. H., crack deflection at an interface between dissimilar elastic materials. *Int. J. Solids Structures*, 1989, **25**, 1053–1067.
10. Phillipps, A. J., Clegg, W. J. and Clyne, T. W., Fracture behaviour of ceramic laminates in bending: I. Modelling of crack propagation. *Acta Metall. Mater.*, 1993, **41**, 805–817.
11. Hasselman, D. P. H., Unified theory of thermal shock fracture initiation and crack propagation in brittle ceramics. *J. Am. Ceram. Soc.*, 1969, **52**, 600–604.
12. Hasselman, D. P. H., Thermal stress resistance parameters for brittle refractory ceramics: a compendium. *Am. Ceram. Soc. Bull.*, 1970, **49**, 1033–1037.
13. Wang, H. and Singh, R. N., Thermal shock behavior of ceramics and ceramic composites. *Int. Mater. Rev.*, 1994, **39**, 228–244.
14. Aldridge, M. and Yeomans, J. A., The thermal shock behavior of ductile particle toughened alumina composites. *J. Eur. Ceram. Soc.*, 1998, **19**, 1769–1775.
15. Hirano, T. and Niihara, K., Thermal shock resistance of Si3N4/SiC nanocomposites fabricated from amorphous Si–C–N precursor powders. *Mater. Lett.*, 1996, **26**, 285–289.
16. Vandeperre, L. J., Kristofferson, A., Carlström, E. and Clegg, W. J., Thermal shock of layered ceramic structures with crack-deflecting interfaces. *J. Am. Ceram. Soc.*, 2001, **84**, 104–110.
17. Lee, W. J. and Case, E. D., Cyclic thermal shock in SiC-whisker reinforced alumina composite. *Mater. Sci. Eng.*, 1989, **A119**, 113–126.
18. Schneibel, J. H., Sabol, S. M., Morrison, J., Ludeman, E. and Carmichael, C. A., Cyclic thermal shock resistance of several advanced ceramics and ceramic composites. *J. Am. Ceram. Soc.*, 1998, **81**, 1888–1892.
19. Lienard, S. Y., Kovar, D., Moon, R. J., Bowman, K. J. and Halloran, J. H., Texture development in Si_3N_4/BN fibrous monolithic ceramics. *J. Mater. Sci.*, 2000, **35**, 3365–3371.
20. 494-92a Standard Practice for Measuring Ultrasonic Velocity in Materials. In *Annual Book of ASTM Standards, Section 3, Vol. 03, Nondestructive Testing Methods,* ed. P. C. Fazio et al. American Society for Testing and Materials, Philadelphia, PA, 1994, pp. 179–190.
21. Hampshire, S., Nitride ceramics. In *Engineered Materials Handbook, Vol. 4, Ceramics and Glasses*. ASM International, 1991, pp. 814–820.
22. Killey, A. and MacMillan, N. H., *Strong Solids, 3 ed.* Oxford University Press, 1986.
23. Koh, Y. H., Kim, H. W. and Kim, H. E., Mechanical properties of fibrous monolithic Si_3N_4/BN ceramics with different cell boundary thicknesses. *J. Ecers. Ceram. Soc.* (in press).
24. Kelly, B. T., The anisotropic thermal expansion of boron nitride II. Interpretation by the semi-continuum model. *Phil. Mag.*, 1975, **32**, 859–867.
25. Yates, B., Ovary, M. J. and Pirgon, O., The anisotropic thermal expansion of boron nitride I. Experimental results and their analysis. *Phil. Mag.*, 1975, **32**, 847–857.
26. Goeuriot-Launay, D., Brayet, G. and Thevenot, F., Boron nitride effect on the thermal shock resistance of an alumina based ceramic composite. *J. Mater. Sci. Lett.*, 1986, **5**, 940–942.
27. Lutz, E. H. and Swain, M. V., Fracture toughness and thermal shock behavior of silicon nitride–boron nitride ceramics. *J. Am. Ceram. Soc.*, 1992, **75**, 67–70.